

# Mechanistic Insights into the Anti-Glioma Effects of Exosome-Like Nanoparticles Derived from *Garcinia Mangostana* L.: A Metabolomics, Network Pharmacology, and Experimental Study

Xuling Luo<sup>1,\*</sup>, Xiaoting Zhang<sup>1,\*</sup>, Aibo Xu<sup>2,3,\*</sup>, Yimin Yang<sup>1b,2,3</sup>, Wei Xu<sup>1b,3</sup>, Min Cai<sup>4</sup>, Peng Xu<sup>1b,5</sup>, Zhen Wang<sup>1b,2,3</sup>, Youmin Ying<sup>1</sup>, Kaiqiang Li<sup>1b,2,3</sup>

<sup>1</sup>College of Pharmaceutical Sciences, Zhejiang University of Technology, Hangzhou, Zhejiang, 310014, People's Republic of China; <sup>2</sup>Center for Laboratory Medicine, Allergy Center, Department of Transfusion Medicine, Zhejiang Provincial People's Hospital (Affiliated People's Hospital), Hangzhou Medical College, Hangzhou, Zhejiang, 310014, People's Republic of China; <sup>3</sup>Key Laboratory of Biomarkers and In Vitro Diagnosis Translation of Zhejiang Province, Hangzhou, Zhejiang, 310063, People's Republic of China; <sup>4</sup>Hangzhou Zhongmeihuadong Pharmaceutical Co., Ltd, Hangzhou, 310011, People's Republic of China; <sup>5</sup>Department of Clinical laboratory, The Third Affiliated Hospital of Zhejiang Chinese Medical University, Hangzhou, Zhejiang, 310011, People's Republic of China

\*These authors contributed equally to this work

Correspondence: Youmin Ying; Kaiqiang Li, Email ymying@zjut.edu.cn; likaiqiang@hmc.edu.cn

**Introduction:** *Garcinia mangostana* L. a widely used tropical fruit, has been historically valued as a medicinal plant. Modern pharmacological research has identified several compounds in its pericarp, such as alkaloids, flavonoids, and phenolic acids, which possess antioxidant and anticancer properties. Recent studies have shown that various medicinal and edible plant-derived nanovesicles (MEPNs) exhibit potent anti-tumor effects. However, the impact of *Garcinia mangostana* L.-derived exosome-like nanoparticles (GELNVs) in treating glioma remains insufficiently explored.

**Methods:** GELNVs were isolated from the rind of *Garcinia mangostana* L. using an environmentally sustainable method. The chemical composition of GELNVs was systematically characterized through both qualitative and quantitative analyses via UPLC-MS/MS. Network pharmacology was utilized to identify potential anti-glioma targets, with a focus on the PI3K-Akt signaling pathway. Subsequently, in vitro experiments were conducted to assess the uptake of GELNVs by glioma cells and their anti-tumor effects, including apoptosis induction, cell proliferation suppression, and effects on microglial polarization.

**Results:** Using a sustainable extraction method, GELNVs were successfully isolated and chemically characterized by UPLC-MS/MS. Network pharmacology and molecular docking identified key anti-glioma targets, particularly AKT1 within the PI3K-Akt signaling pathway. In vitro experiments demonstrated that GELNVs were effectively internalized by GL261 glioma and BV2 microglial cells, showing significant anti-glioma activity by inducing apoptosis and inhibiting cell proliferation. Additionally, GELNVs promoted the activation of M1-type microglia while inhibiting M2 polarization induced by IL-4 and glioma cells. This was evidenced by the upregulation of inflammatory mediators, including iNOS, TNF- $\alpha$ , IL-6, and IL-1 $\beta$  at the mRNA level.

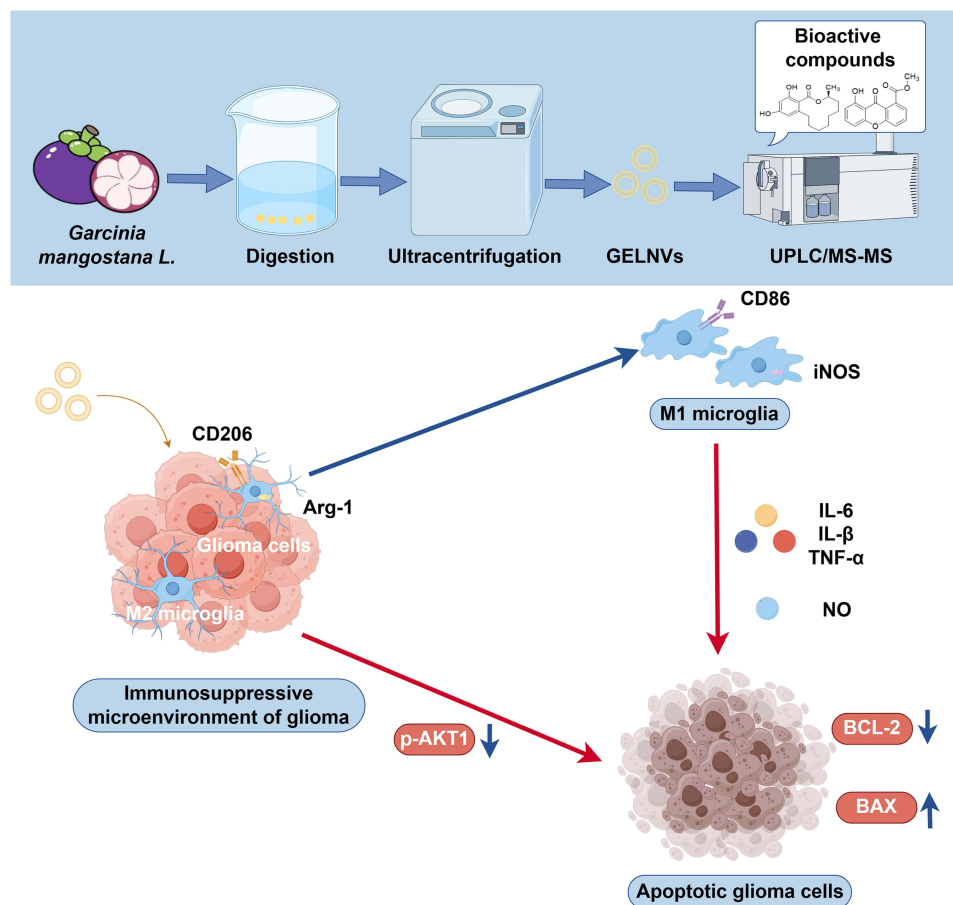
**Conclusion:** Our findings demonstrate that GELNVs represent a potential therapeutic strategy for glioma by inducing apoptosis in tumor cells and inhibiting their proliferation through suppression of the PI3K-Akt signaling pathway. Furthermore, GELNVs show promise in modulating microglial polarization, further highlighting their potential as a glioma treatment.

**Keywords:** plant-derived exosome-like nanoparticles, glioma, microglia, Akt, network pharmacology, molecular docking

## Introduction

Glioma is a highly heterogeneous and aggressive form of primary malignant tumor in the central nervous system, accounting for 30% to 50% of all primary brain neoplasms.<sup>1,2</sup> Its high recurrence rate and low 5-year survival rate pose a serious threat to human health.<sup>3</sup> Temozolomide (TMZ), the first-line chemotherapy drug and a precursor alkylating agent

## Graphical Abstract



for glioma, is widely used due to its stability, solubility, oral availability, and ability to cross the blood-brain barrier (BBB).<sup>4,5</sup> However, the development of drug resistance and associated toxic side effects severely limit its therapeutic efficacy,<sup>6</sup> emphasizing the need for more effective treatment options. In contrast to other solid malignancies, the glioma microenvironment is characterized by a highly immunosuppressive phenotype with notable absence of T-cell infiltration.<sup>7</sup> Immunotherapeutic strategies targeting the glioma immune microenvironment, including immune checkpoint inhibitors, oncolytic viruses, cancer vaccines, and CAR-T cell therapies, represent a promising avenue for advancing glioma treatment.<sup>8</sup> Microglia, as resident immune cells in the brain, represent potential therapeutic targets for glioma immunotherapy.<sup>9</sup> The glioma microenvironment is predominantly populated by M2-polarized microglia, which promote tumor progression, angiogenesis, and invasion through secretion of cytokines including IL-10 and TGF- $\beta$ , whereas M1-polarized microglia exhibit tumor-suppressive functions.<sup>10</sup> In summary, the concurrent cytotoxic targeting of tumor cells and reprogramming of microglia towards an M1-polarized phenotype represents a promising therapeutic strategy.

Accumulating evidence suggests that exosomes are involved in the pathogenesis and progression of tumors, sourced from various organisms including animals,<sup>11</sup> plants,<sup>12</sup> and microbes.<sup>13</sup> Exosomes possess unique properties such as high bioavailability, the ability to penetrate the BBB, and low immunogenicity, making them promising candidates for cancer therapy. Recent studies have highlighted the therapeutic potential of natural compounds in addressing human diseases. Specifically, significant progress has been made in the development of medical and edible plant-derived nanovesicles (MEPNs). MEPNs are a class of lipid bilayer-enclosed nanovesicles isolated from medicinal and edible plants through methodologies encompassing polyethylene glycol precipitation, ultracentrifugation, size-exclusion chromatography, and

so on.<sup>14</sup> These nanostructures encapsulate bioactive constituents including proteins, lipids, RNA, and active compounds, and are actively involved in multifaceted physiological processes such as intercellular communication, tumorigenesis and metastasis, and immune responses.<sup>15</sup> MEPNs have been extracted from numerous common plants, such as grapes, lemons, ginger, garlic, *Catharanthus roseus*, and tea leaves.<sup>16–19</sup> Due to the varying active components in these plants, MEPNs exhibit distinct biological functions and therapeutic effects. For instance, Zhao et al demonstrated that garlic-derived exosome-like nanovesicles, rich in amino acids and their derivatives, alleviate acute liver failure by inhibiting CCR2/CCR5 signaling and suppressing NLRP3 inflammasome activation.<sup>20</sup> Similarly, Chen et al found that tea leaf-derived exosome-like nanoparticles, abundant in polyphenols and flavonoids, induce the generation of reactive oxygen species and promote apoptosis in tumor cells.<sup>16</sup> Ginseng-derived exosome-like nanoparticles, notable for their ginsenoside content, have been shown to enhance BBB penetration and modulate the tumor microenvironment, making them valuable for cancer treatment.<sup>21</sup> Furthermore, MEPNs demonstrate superior therapeutic efficacy in disease treatment compared to isolated single active compounds from the same botanical source.<sup>22</sup> This enhanced performance is primarily attributable to the nanoscale dimensions and membrane architecture of MEPNs, which collectively improve the bioavailability of encapsulated active components and enable synergistic interactions among multiple constituents.<sup>18</sup> Moreover, MEPNs exhibit reduced immunogenicity and enhanced stability, thereby establishing a crucial foundation for their clinical translation.<sup>23</sup>

*Garcinia mangostana* L., traditionally used to treat various diseases such as cancer, pain, neurodegeneration, diabetes, and hyperlipidemia,<sup>24,25</sup> has garnered attention for its potent pharmacological properties. Our previous research demonstrated that a  $\beta$ -mangostin derivative from *Garcinia mangostana* L. exhibits anti-glioma properties, along with fostering an immune microenvironment that inhibits glioma growth.<sup>26</sup> Given these promising findings, it is anticipated that exosome-like nanoparticles derived from *Garcinia mangostana* L. (GELNVs) would also carry various bioactive components, including flavonoids (eg, quercetin and its derivatives) and oxygenated anthraquinones (eg,  $\beta$ -mangostin). Metabolomics is a research approach that conducts quantitative analysis of all metabolites in an organism and seeks the relative relationships between metabolites and physiological and pathological changes.<sup>27</sup> Notably, the metabolomics technology analysis has been proven to be highly effective for the identification of plant metabolites and the elucidation of pathways in primary and secondary plant metabolism.<sup>28</sup> To investigate the bioactive components in GELNVs, this study isolated and detected small molecule compounds in GELNVs using a UPLC-ESI-MS/MS system and performed identification by comparing with the self-constructed Metware Database (MWDB). MWDB is a manually curated metabolite repository constructed through systematic integration of authentic chemical standards, public metabolite databases, and literature-derived spectral data. This knowledgebase employs advanced UPLC-ESI-MS/MS fragmentation pattern analysis, incorporating both collision-induced dissociation (CID) and higher-energy collisional dissociation (HCD) profiles, to establish validated spectral libraries for confident metabolite annotation.

In this study, GELNVs were successfully isolated through continuous differential centrifugation and ultracentrifugation. An integrated approach combining metabolomics, network pharmacology, and experimental validation was employed to evaluate the therapeutic potential of GELNVs against glioma cells. We found that nano-sized GELNVs, containing a variety of chemical cargoes, promote apoptosis and inhibit proliferation in GL261 glioma cells via the PI3K/Akt signaling pathway. Additionally, GELNVs were shown to remodel the function of M2-type microglia induced by IL-4 and glioma cells, reactivating the anti-tumor immune response, contributing to an effective anti-glioma effect.

## Materials and Methods

### Isolation of GELNVs

*Garcinia mangostana* L. was purchased from a farmer's market in Hangzhou, China. The fruit was thoroughly washed to remove any dirt, and the red pulp of the rind was chopped and soaked in cold PBS (pH 7.4). It was then digested with pectinase (Scientific Phygene, Fuzhou, China) (0.2 g/100 mL) and cellulase (2 g/100 mL).<sup>29</sup> The pH was adjusted to 7.4, and the mixture was blended at high speed for 5 minutes, with a 1-minute pause after every minute of blending, to produce *Garcinia mangostana* L. juice. The obtained juice was filtered to remove plant residues and then centrifuged sequentially at  $3000 \times g$  for 30 minutes,  $15,000 \times g$  for 60 minutes, and finally ultracentrifuged at  $120,000 \times g$  for 90

minutes.<sup>30</sup> The resulting pellets were diluted with PBS and centrifuged at  $150,000 \times g$  for 120 minutes using a sucrose density gradient (8%, 15%, 30%, 45%, 60%) in 0.02M Tris-HCl to purify GELNVs.<sup>31</sup> The final solution was washed twice to remove sucrose, re-suspended in cold Tris-HCl, filtered through a 0.22  $\mu\text{m}$  filter to obtain sterile GELNVs, and stored at  $-80^\circ\text{C}$  for further characterization.

## Characterization of GELNVs

10  $\mu\text{L}$  sample was deposited onto a 2 mm copper grid and allowed to settle for 10 minutes until complete air-drying. Subsequently, negative staining was performed by applying 3% phosphotungstic acid solution to the grid for 5 minutes. The prepared specimen was then subjected to morphological characterization through transmission electron microscopy (Hitachi, Tokyo, Japan) operating at an accelerating voltage of 90 Kv.<sup>11</sup> Size distribution and zeta potential were analyzed via dynamic light scattering (DLS) using a Zetasizer Nano ZSE (Malvern Instruments, UK). Protein concentrations were measured with the BCA Protein Quantification Assay Kit (Thermo Fisher Scientific, Waltham, MA, USA), using bovine serum albumin as the standard.

## Composition Analysis of GELNVs

Take the sample for vacuum freeze-drying. Then add 80% methanol internal standard extract precool at  $-20^\circ\text{C}$ , vortex for 2 minutes. The samples are subjected to freezing and thawing using liquid nitrogen, repeated 3 times. Centrifuge at 12000 r/minutes for 10 minutes at  $4^\circ\text{C}$ . Finally, extract the supernatant, filter it with a microporous filter membrane (0.22  $\mu\text{m}$ ), and store it in the injection bottle for LC-MS/MS detection. The chemical composition of GELNVs was analyzed using an ultra-performance liquid chromatography (UPLC, ExionLC™ AD, <https://sciex.com.cn/>) system coupled with a tandem mass spectrometry (MS/MS, QTRAP® 6500+ System, <https://sciex.com>) system.<sup>32</sup> The UPLC column used was SB-C18 (1.8  $\mu\text{m}$ , 2.1 mm  $\times$  100 mm, Agilent). The mobile phase consisted of phase A (ultrapure water with 0.1% formic acid) and phase B (acetonitrile with 0.1% formic acid). The column temperature was maintained at  $40^\circ\text{C}$ , with an injection volume of 2  $\mu\text{L}$ . Mass spectrometric analysis was conducted using a triple quadrupole mass spectrometer in multiple reaction monitoring (MRM) mode.

The electrospray ionization (ESI) source was set to a temperature of  $550^\circ\text{C}$ , with an ion spray voltage of 5500 V (positive ion mode) or  $-4500$  V (negative ion mode). The nebulizer gas (GS1) was set to 50 psi, turbo-gas (GS2) to 60 psi, and curtain gas (CUR) to 25 psi.

## Metabolite Qualitative and Quantitative Analysis

Utilizing the self-constructed MWDB V4.4 (Metware Biotechnology Co., Ltd. Wuhan, China) for compound identification, we conducted qualitative analysis based on secondary mass spectral data. During this process, isotopic signals, redundant signals containing  $\text{K}^+$ ,  $\text{Na}^+$ , and  $\text{NH}_4^+$  ions, as well as redundant fragment ion signals originating from larger molecules, were excluded. Quantitative analysis was performed using the multiple reaction monitoring (MRM) mode on a triple quadrupole mass spectrometer.

## Screening of GELNVs for Potential Active Ingredients and Collection of Related Targets

Based on the chemical composition of GELNVs obtained through UPLC-MS/MS, the compounds were queried using the PubChem database (<https://pubchem.ncbi.nlm.nih.gov/>). The corresponding simplified molecular input line entry system (SMILES) strings were then downloaded, and these SMILES strings were imported into the online Swiss ADME database (<http://www.swissadme.ch/>) to further screen for active ingredients and predict their ADME parameters. The screening criteria were as follows: high gastrointestinal (GI) absorption for pharmacokinetic selection, BBB permeability, and three or more compounds with “YES” in the five drug-likeness rules (Lipinski, Ghose, Veber, Egan, Muegge) can be regarded as active ingredients. It is indicated that compounds adhering to the five drug-likeness rules exhibit superior pharmacokinetic properties, demonstrating higher bioavailability during metabolic processes within biological organisms, and therefore are more likely to become oral medications.<sup>33</sup> Lipinski/Ghose: Limits molecular size and lipid



solubility to ensure that compounds can penetrate cell membranes; Veber/Egan: Drug Absorption and Bioavailability; Muegge: Further rule out structures that are difficult to drug; Violation of the Muegge principle may indicate a toxic hazard.<sup>34</sup> Compounds that satisfied both conditions were considered active. The SMILES strings of the active ingredients were subsequently imported into the Swiss TargetPrediction database (<http://swisstargetprediction.ch/>) for target prediction, and compounds with a predicted probability  $\geq 0.1$  were considered relevant targets for GELNVs.

## Screening of Targets of GELNVs Against Glioma

Glioma-related targets were identified using the GeneCards (<https://www.genecards.org/>), DisGeNet (<https://www.disgenet.org/>), and BrainBase (<https://ngdc.cncb.ac.cn/brainbase/index>) databases. After removing duplicates and filtering the results, a glioma-related target database was constructed. To ensure result accuracy, we selected targets from the DisGeNet and GeneCards databases with a score  $\geq 0.5$  and a relevance score  $\geq 5$ . The targets related to GELNVs were then intersected with the disease-related targets using Venny 2.1.0 (<http://www.liuxiaoyu.com/>). The intersecting targets were mapped to identify the anti-glioma targets of GELNVs.

## Analysis of Protein-Protein Interactions

Protein-protein interactions (PPI) reveal the relationships between different proteins. The identified intersecting genes were imported into the Search Tool for the Retrieval of Interaction Gene/Proteins (STRING) database (<https://cn.string-db.org/>), with the species set to Homo sapiens and a confidence score  $\geq 0.4$ , while unrelated nodes were hidden. The data were then visualized using Cytoscape 3.9.1, resulting in a PPI network diagram. Centiscape 2.2 (a plug-in for Cytoscape) was used to calculate three topological network parameters for each node: Closeness, Degree, and Betweenness. The nodes were filtered based on their Degree values, and the top 10 targets were considered the key targets of GELNVs for glioma treatment. Nodes with higher parameter values were identified as more significant, leading to the construction of a refined PPI network.

## Gene Ontology (GO) and Kyoto Encyclopedia of Genes and Genomes (KEGG) Pathway Enrichment Analysis

To investigate the biological functions and pathways involved in the anti-glioma effects of GELNVs, Gene Ontology (GO) and Kyoto Encyclopedia of Genes and Genomes (KEGG) pathway enrichment analyses were performed to explore the core mechanisms and pathways of all potential targets. The intersecting genes were imported into the Database for Annotation, Visualization and Integrated Discovery (DAVID) database (<https://david.ncifcrf.gov/>) to predict gene functions across Molecular Function (MF), Biological Process (BP), Cellular Component (CC), and KEGG pathways. The results were visualized using the online tool (<http://www.bioinformatics.com.cn/>).

## Molecular Docking

The binding efficacy between the active compounds in GELNVs and the core target was analyzed using molecular docking techniques. Structural files for both receptors and ligands were sourced, with ligand structure data file (SDF) structures retrieved from the PubChem database and 3D structures of receptors obtained from the Research Collaboratory for Structural Bioinformatics Protein Data Bank (RCSB PDB) database (<https://www.rcsb.org/>). Subsequent processing of the ligands involved the addition of hydrogen atoms and charge assignment. Receptor proteins were prepared through dehydration, ligand removal, and the definition of docking sites. AutoDock Tools 1.5.6 was utilized to perform the docking simulations. Typically, a docking energy below  $-5$  kcal/mol was considered indicative of binding affinity between the target and the compound.<sup>35</sup> Pymol 2.4.0 was employed to visualize the docking results, ensuring a comprehensive analysis of the interactions between the components of GELNVs and the core targets.

## Uptake of GELNVs

Efficient cell internalization of GELNVs is a prerequisite for exerting anti-tumor effects. GL261 or BV2 cells were seeded into 24-well plates with a density of  $5 \times 10^4$  cells per well. To detect the direct transfer of GELNVs into cells, the

GELNVs were labeled with the DiI dye and incubated with BV2 and GL261 cells for 24 hours. The fluorescence signals were then detected using a confocal microscope equipped with a digital image analysis system (Leica, Wetzlar, Germany).

## Cell Viability Assay

Cell viability was assessed using the CCK-8 assay. GL261 or BV2 cells were seeded into 96-well plates with a density of 5000 cells per well. Cells were incubated with varying concentrations of GELNVs (0, 25, 50, 100, 150, 200, 300, and 400  $\mu\text{g/mL}$ ) for 24 hours. After the incubation period, 10  $\mu\text{L}$  of CCK-8 solution (Vazyme, Nanjing, China) was added to each well, followed by an additional 2-hour incubation. Absorbance was then measured at 450 nm using a microplate reader (Biotek, Winooski, VT, USA).

## Cell Proliferation Assay

Cell proliferation was detected by the EdU assay. GL261 cells were seeded into 24-well plates with a density of  $5 \times 10^4$  cells per well. Cells were incubated with 5  $\mu\text{M}$  doxorubicin (DOX), 17.82  $\mu\text{M}$   $\beta$ -mangostin ( $\beta$ -mgs), and varying concentrations of GELNVs (50, 100, and 200  $\mu\text{g/mL}$ ) for 24 hours.<sup>26,36</sup> After the incubation period, 10  $\mu\text{M}$  of EdU solution (Beyotime, Shanghai, China) was added to each well, followed by an additional 2-hour incubation. The Click Additive Solution is then formulated and added to each well. Finally, EdU staining was observed under a fluorescence microscope (Invitrogen, Carlsbad, CA, USA).

## Cell Migration Assay

Cell Migration was detected by the wound healing assay. GL261 cells were seeded into 24-well plates with a density of  $6 \times 10^5$  cells per well and allowed to grow to 90% confluence. 200  $\mu\text{L}$  pipetting head was used to scratch the cells in the plate. Cells were incubated with 5  $\mu\text{M}$  doxorubicin (DOX), 17.82  $\mu\text{M}$   $\beta$ -mangostin ( $\beta$ -mgs), and varying concentrations of GELNVs (50, 100, and 200  $\mu\text{g/mL}$ ) for 24 hours. Collect images under an inverted microscope (Olympus, Tokyo, Japan) at 0 h and 24 h.

## Cellular Apoptosis Assay by Flow Cytometry

Apoptosis of GL261 glioma cells was assessed using an Annexin V-FITC apoptosis detection kit (Lianke, Hangzhou, China) following the manufacturer's protocol. GL261 cells were seeded into 6-well plates with a density of  $4 \times 10^5$  cells per well. After 24 hours of incubation with 100  $\mu\text{g/mL}$  GELNVs, the cells were washed three times with pre-cooled PBS, trypsinized, and collected by centrifugation at  $1000 \times \text{rpm}$  for 3 minutes. The cells were then resuspended in Binding Buffer, and 5  $\mu\text{L}$  of Annexin V-FITC and 10  $\mu\text{L}$  of PI were added. The mixture was gently vortexed and incubated in the dark at room temperature for 5 minutes. Fluorescence intensity at the corresponding wavelengths was quantitatively measured using flow cytometer (Agilent Technologies, Santa Clara, CA, USA).

## Western Blotting

Total proteins were extracted from GL261 cells treated with 50, 100, and 200  $\mu\text{g/mL}$  GELNVs and 4  $\mu\text{g/mL}$  SC79. Proteins from each sample were separated by SDS-PAGE and transferred to PVDF membranes, which were blocked with 5% non-fat dry milk for 2 hours. The membranes were then incubated overnight at  $4^\circ\text{C}$  with the primary antibody (HUABIO, Hangzhou, China): AKT1 (ET1609-47), p-AKT1 (ET1607-73), BAX (ET1603-34), BCL-2 (ET1702-53), and GAPDH (ET1601-4). After washing with TBST, membranes were incubated with HRP-coupled secondary antibody (HUABIO, Hangzhou, China). Specific protein bands were detected using a chemiluminescence and gel imaging system (Bio-Rad, USA).

## Co-Culture

BV2 cells were cultured in the lower chamber of Transwell™ 6-well chambers (Corning, NY, USA) with a density of  $4 \times 10^5$  cells per well. Then, GL261 cells were seeded into the upper chamber with a density of  $2 \times 10^5$  cells per well. After

24 hours of incubation with 100 µg/mL GELNVs, BV2 cell supernatants and cells were collected for NO, PCR, and flow cytometry detection.

## Quantitative Real-Time PCR

Cells were collected and lysed using Trizol reagent for RNA extraction, followed by reverse transcription to synthesize cDNA. Quantitative real-time polymerase chain reaction (PCR) was conducted on an Applied Biosystems 7500 Real-Time PCR system (Applied Biosystems, Waltham, MA, USA). The primers used in the PCR were synthesized by Sunya Biotech Corporation (Hangzhou, China), and the details of the primers utilized in this study are provided in [Supplementary Table 1](#).

## Microglia Polarization Assay by Flow Cytometry

Cells were stained with Fixable Viability Stain 510 (BD Bioscience, San Diego, CA, USA) and blocked with Fc block in turn, followed by incubation with anti-CD11b and anti-CD86 (BioLegend, San Diego, CA, USA). After fixation/permeabilization, cells were stained with anti-CD206. Cell fluorescence was analyzed using flow cytometer (Agilent Technologies, Santa Clara, CA, USA).

## Statistical Analysis

Data analysis for this study was conducted using GraphPad Prism 9.5 software (CA, USA). Trials were performed three times, and outcomes were articulated as mean ± standard deviation. The Shapiro–Wilk test was used to determine whether the data were normally distributed. If the data conform to a normal distribution, the statistical mean difference was assessed using an unpaired *t*-test or one-way ANOVA to determine significance. Significant changes were defined as  $*p < 0.05$  and extremely significant changes as  $**p < 0.01$ .

## Results

### Physicochemical Characterization of GELNVs

To achieve a high degree of purification for GELNVs, we employed a multi-step process involving pectinase and cellulase digestion, ultrafiltration, and sucrose density gradient centrifugation for nanovesicle isolation ([Figure 1A](#)). The distribution of various sucrose density layers is shown in [Figure 1B](#), revealing nanoparticle accumulation in the 8–15% (G1), 15–30% (G2), and 30–45% (G3) sucrose solutions. The particle sizes of GELNVs from these layers increased with density, all remaining below 200 nm in diameter, in accordance with the 2023 guidelines of the International Society for Extracellular Vesicles (MISEV2023).<sup>37</sup> Specifically, the size distributions for G1, G2, and G3 were 66.8 nm, 90.5 nm, and 102.5 nm, respectively ([Figure 1D](#)). The zeta potentials of the GELNVs were measured at −7.93 mV for G1, −4.81 mV for G2, and −4.05 mV for G3 ([Figure 1C](#)), consistent with the negative potential characteristic of exosomes. Notably, further morphological analysis using transmission electron microscopy (TEM) revealed typical cup-shaped exosome structures with minimal impurities in G3, which was subsequently selected for follow-up experiments ([Figure 1E–G](#)). These results demonstrate the successful isolation of structurally intact, exosome-like nanoparticles derived from *Garcinia mangostana* L.

### Composition Analysis of GELNVs

To investigate the biological and pharmacological properties of GELNVs, we employed a comprehensive targeted metabolomics strategy using UPLC-MS/MS to elucidate their chemical composition. Metabolite detection and analysis were performed in both positive and negative ionization modes. The superimposed total ion chromatograms (TIC) of pooled quality control (QC) samples, along with the constructed multiple reaction monitoring (MRM) chromatograms, demonstrated consistent retention times and peak intensities, indicating high reproducibility. This stability ensures the repeatability and reliability of the data, providing critical assurance for research outcomes ([Supplementary Figure 1](#)). The total ion chromatograms of the samples in both positive and negative ion modes revealed the full composition of GELNVs ([Figure 2A and B](#)). In total, 1,555 compounds were identified and categorized into 12 distinct classes

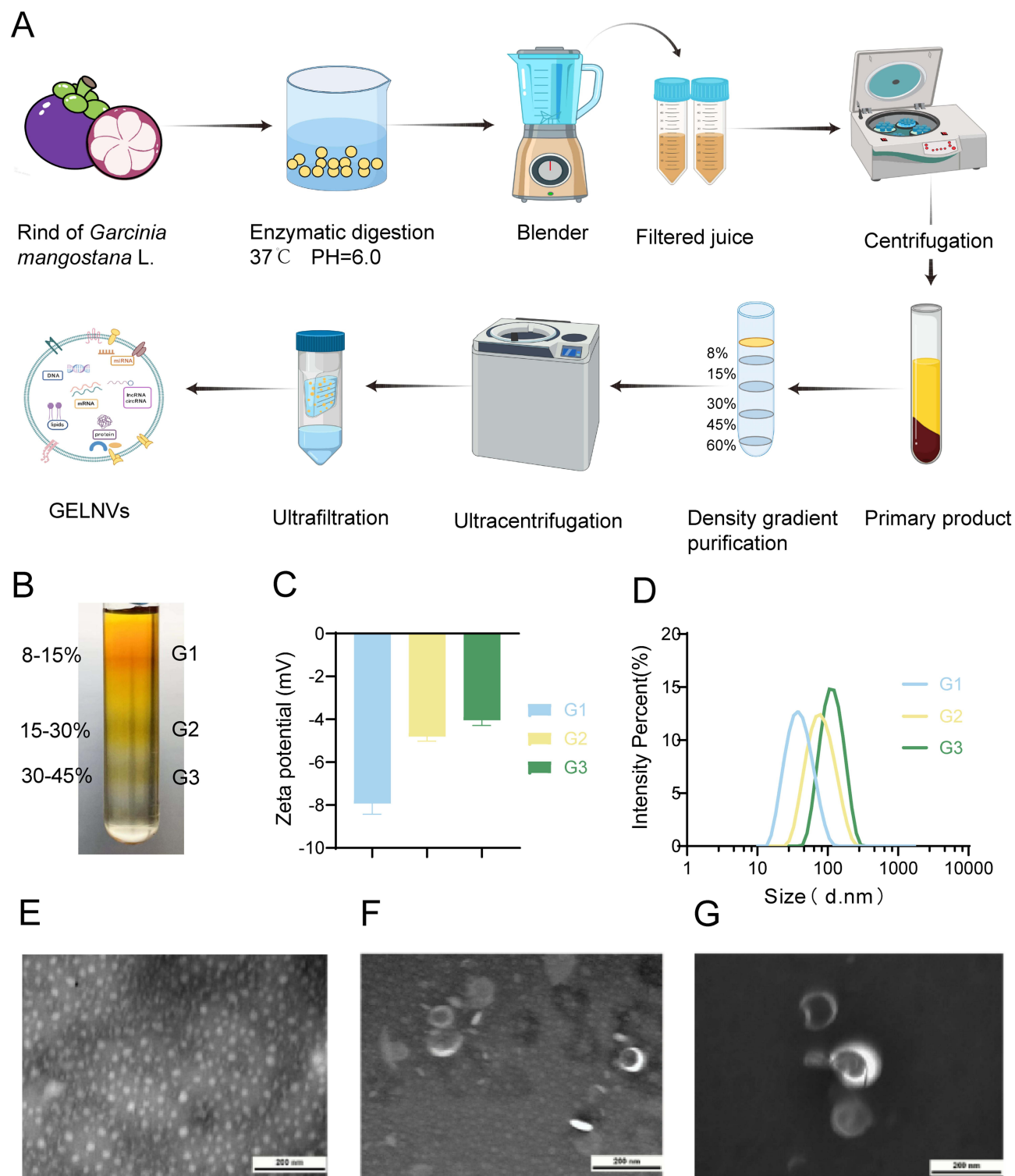
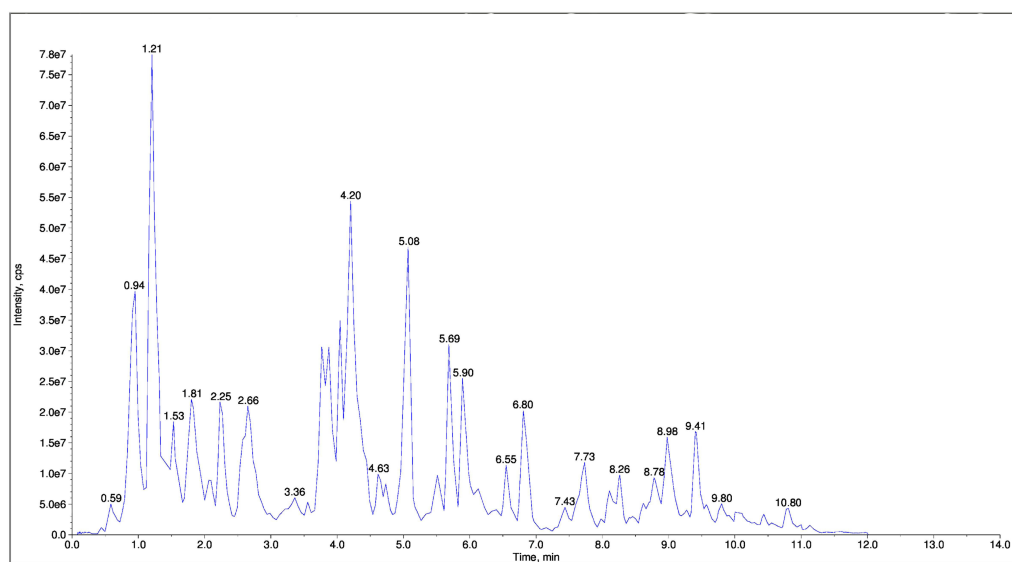


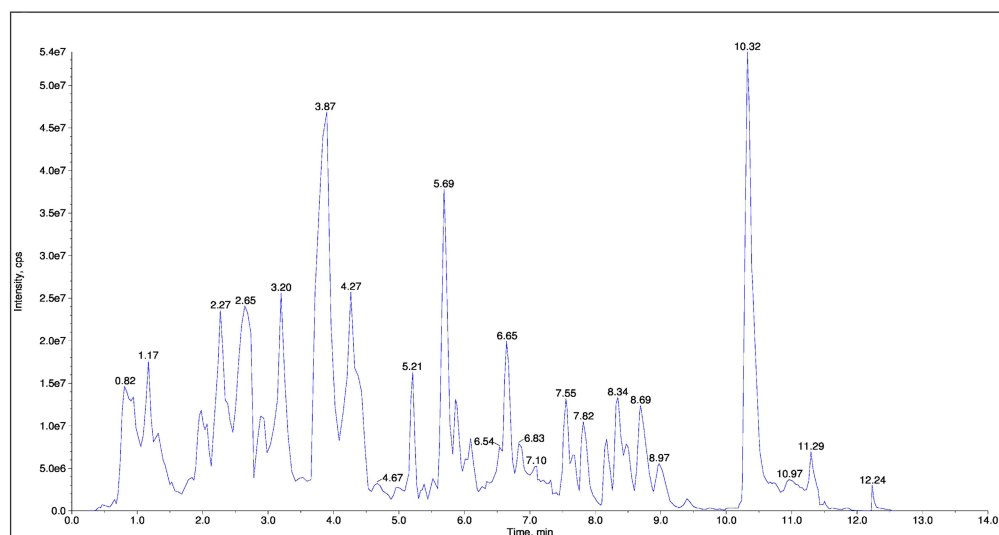
**Figure 1** Isolation and physicochemical characterization of GELNVs. **(A)** Schematic illustration of the isolation process of GELNVs. **(B)** Distribution images of GELNVs after sucrose density gradient purification. **(C, D)** DLS was used to analyze the zeta potential and size distribution of GELNVs. **(E–G)** TEM image of GELNVs at different sucrose concentrations (From left to right: G1, G2 and G3, scale bars=200 nm).

(Figure 2C). Notably, the top 200 compounds, ranked by relative abundance, accounted for 95.28% of the total compounds identified, prompting their selection for further analysis (Supplementary Table 2). These predominant compounds were primarily flavonoids, amino acids and their derivatives, alkaloids, and phenolic acids (Figure 2D).

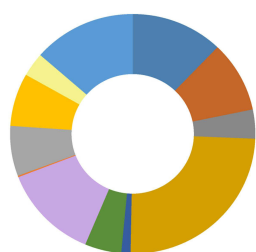
A



B

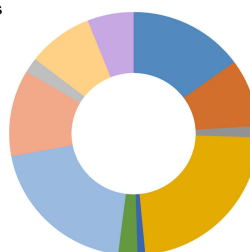


C



- 12.16% Amino acids and derivatives  
 ■ 9.58% Phenolic acids  
 ■ 3.92% Nucleotides and derivatives  
 ■ 24.63% Flavonoids  
 ■ 1.22% Quinones  
 ■ 4.82% Lignans and Coumarins  
 ■ 12.7% Others  
 ■ 0.2% Tannins  
 ■ 6.75% Alkaloids  
 ■ 7.14% Terpenoids  
 ■ 3.22% Organic acids  
 ■ 13.57% Lipids

D



- 15% Amino acids and derivatives  
 ■ 9% Phenolic acids  
 ■ 1.5% Nucleotides and derivatives  
 ■ 23% Flavonoids  
 ■ 1% Quinones  
 ■ 2.5% Lignans and Coumarins  
 ■ 20% Others  
 ■ 11.5% Alkaloids  
 ■ 2% Terpenoids  
 ■ 8.5% Organic acids  
 ■ 6% Lipids

**Figure 2** Metabolomic analysis of GELNVs. Total ion flow diagrams for the GELNVs positive (A) and negative (B) ion models. (C) The relative content classification ratio of all GELNVs components. (D) The classification ratio of the top 200 GELNVs components.



## Screening of Active Components and Target Predictions

Based on the drug target database, a total of 434 potential target genes associated with the active components of GELNVs were predicted. Additionally, 503 glioma-related target genes were retrieved from the disease target database. A Venn diagram revealed 45 overlapping targets between GELNVs and glioma, which were identified as potential therapeutic targets for GELNVs in glioma treatment (Figure 3A). These common targets were imported into Cytoscape 3.9.1 software to construct a visual network of GELNVs-active components-key targets-glioma, excluding components without intersections (Figure 3B and C).

Network topology analysis indicated that butyl isobutyl phthalate, disobutyl phthalate, danthron, lauryldiethanolamine, embelin, azelaic acid, des-o-methylsalsolidipodin, dibutyl phthalate, abscisic acid, 2-hydroxycinnamic acid, hamiltone A, oleamide, and vertixanthone are the major active components, each connected to multiple targets. This suggests that these compounds likely play significant roles in anti-glioma activity, potentially through multifaceted mechanisms.

To further explore the interactions among these targets and identify core target proteins, the 45 intersecting genes were uploaded to the STRING database. Using Cytoscape 3.9.1 software for topological analysis and visualization, we constructed a PPI network, where larger node sizes represent higher degree values, and deeper colors indicate higher node ranks, signifying greater importance in the network. Centiscape 2.2 in Cytoscape identified 10 potentially significant targets: AKT1, CTNNB1, EGFR, CASP3, BCL-2, CCND1, ERBB2, MMP9, PTGS2, and PPARG (Figure 3D–F, Table 1).

## GO and KEGG Pathway Analysis

The top 10 enriched GO terms ( $p < 0.01$ ) and the top 20 enriched KEGG pathways ( $p < 0.01$ ) are shown in Figure 4. The results indicate that the primary biological processes involve protein phosphorylation, angiogenesis, regulation of cell proliferation, and apoptotic processes (Figure 4A). Additionally, cellular component (CC) enrichment analysis shows that GELNVs predominantly exert their effects in the nucleus, cytoplasm, and cytosol. The molecular functions (MF) mainly include protein binding and kinase activity.

Among the KEGG pathways associated with these targets, GELNVs primarily impact the PI3K-Akt, MAPK, Ras, and Rap1 signaling pathways (Figure 4B). Notably, the cancer pathway and the PI3K-Akt signaling pathway were highly significant, with 26 and 20 intersecting genes, respectively.

## Results of Molecular Docking

Through molecular docking analysis, we selected active compounds from GELNVs to dock with the core target protein (AKT1) (Table 2). The molecular docking energy scores for the 13 active compounds with the key target protein are detailed in Supplementary Table 3. Lower binding energy indicates greater binding stability. The results showed that the active compounds exhibited good binding energies with AKT1. In particular, hamiltone A, des-o-methylsalsolidipodin, and vertixanthone demonstrated the lowest docking energy scores. Figure 5 illustrates the three-dimensional docking conformations of these compounds with the target protein.

## In vitro Cellular Uptake and Anti-Tumor Activities of GELNVs

The biological activity of GELNVs is fundamentally dependent on their cellular uptake. Our results demonstrate that GELNVs were efficiently internalized by both BV2 and GL261 cells, with predominant localization in the cytoplasm (Figure 6A). To assess the impact of GELNVs on apoptosis-related cellular events, we employed various methods. First, cell viability after GELNVs treatment was evaluated in GL261 and BV2 cells using the CCK-8 assay. The IC<sub>50</sub> values were determined to be 148.0 µg/mL for GL261 cells and 450.0 µg/mL for BV2 cells, indicating favorable biocompatibility (Figure 6B). Additionally, the anti-proliferation effects of GELNVs on GL261 glioma cells were quantitatively assessed via EdU assay. As shown in Figure 6C and D, GELNVs inhibit GL261 cell proliferation dose-dependently ( $p < 0.01$ ). Moreover, GELNVs inhibit GL261 cell migration dose-dependently ( $p < 0.01$ , Supplementary Figure 2).

Flow cytometry with Annexin V-FITC/PI staining revealed a higher proportion of apoptotic cells, especially in the late apoptosis stage, in the group treated with 100 µg/mL GELNVs compared to the control ( $p < 0.01$ , Figure 6E and F). To further confirm the induction of apoptosis by GELNVs in GL261 glioma cells, we assessed the protein expression

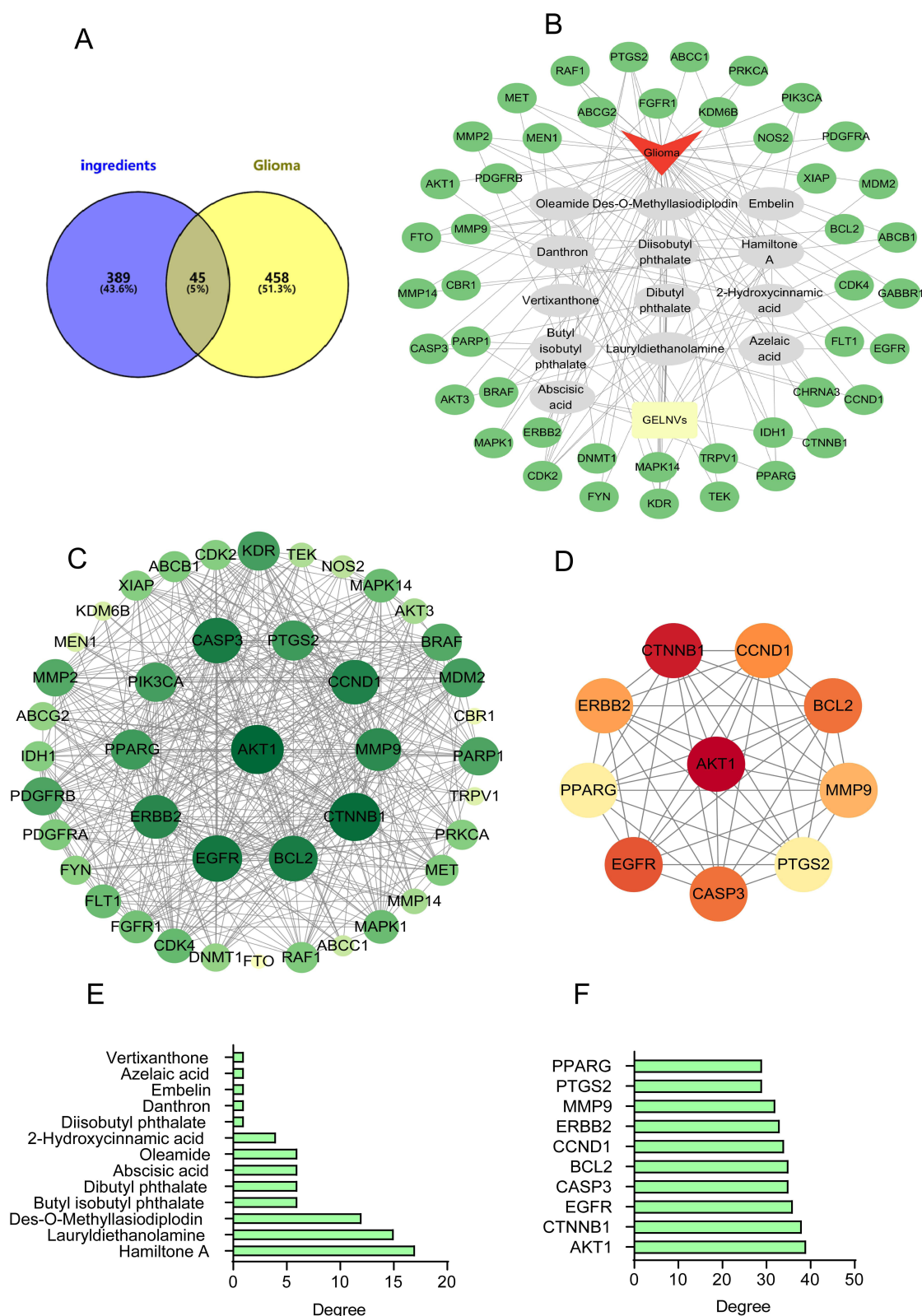
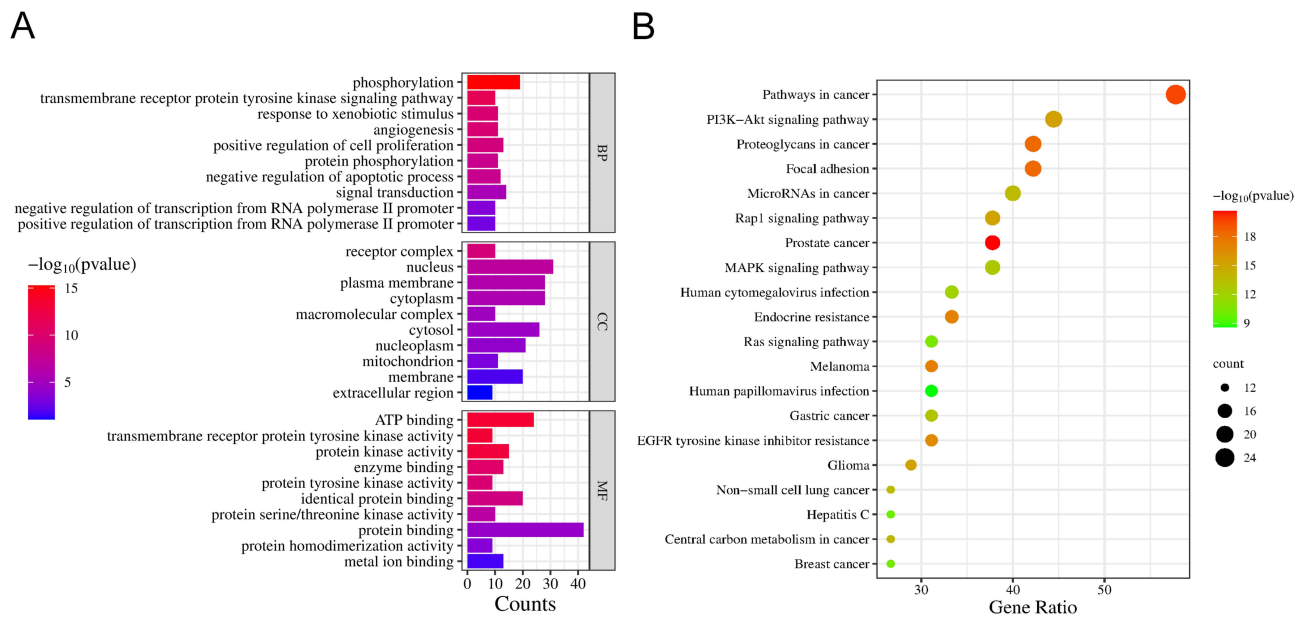


**Table 1** Analysis of the Topological Characteristics of Protein-Protein Interactions. (the top 10 Degrees)

Rank	Name	Betweenness	Closeness	Degree
1	AKT1	109.9453991	0.022222222	39
2	CTNNB1	83.65528366	0.021739130	38
3	EGFR	91.19531388	0.020833333	36
4	CASP3	55.81712933	0.020408163	35
5	BCL2	45.16714402	0.020408163	35
6	CCND1	42.40334312	0.020000000	34
7	ERBB2	37.0795954	0.019607843	33
8	MMP9	32.40028398	0.019230769	32
9	PTGS2	53.55680335	0.018181818	29
10	PPARG	116.9160943	0.018181818	29

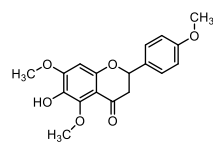
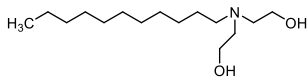
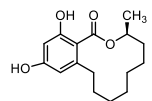
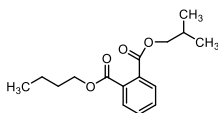
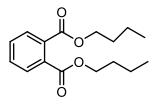
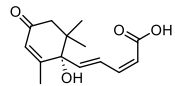
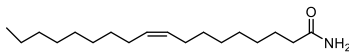
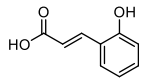
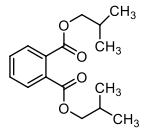
levels of apoptosis-related genes BAX and BCL-2. The results showed an upregulation of BAX and a downregulation of the anti-apoptotic gene BCL-2, indicating that GELNVs promote apoptotic processes in glioma cells.

Network pharmacology analysis suggests that the PI3K-Akt pathway plays a crucial role in GELNVs' anti-glioma effects. To verify this, glioma cells were treated with different concentrations of GELNVs, and AKT1 and p-AKT1 levels were measured via Western blotting. The results demonstrated that GELNVs decreased p-AKT1 levels in glioma cells (Figure 6G). To functionally validate this pathway, rescue experiments were subsequently performed using SC79 (a specific AKT agonist that enhances AKT1 autophosphorylation<sup>38</sup>) to interrogate whether activation of AKT signaling could reverse GELNVs-mediated apoptotic effects. Western blotting analysis revealed that promotion of p-AKT1 via SC79 significantly upregulated BCL-2 expression while concurrently suppressing BAX levels (Supplementary Figure 3). This molecular intervention effectively counteracted the pro-apoptotic effects mediated by GELNVs. These findings further demonstrate that GELNVs induce glioblastoma cell apoptosis through inhibition of AKT1 phosphorylation-dependent pathways (Figure 6H).



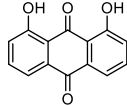
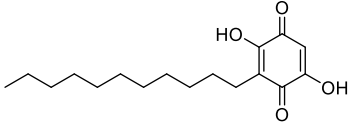
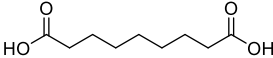
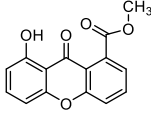
**Figure 4** GO and KEGG enrichment analysis of intersection targets. (A) GO shows the top 10 GO terms for BP, CC and MF ( $p < 0.05$ ). (B) KEGG enrichment analysis of the top 20 signaling pathways ( $p < 0.05$ ).

**Table 2** Information of 13 Active Components From GELNVs

Number	Compounds	Formula	CAS	Structure
1	Hamilton A	$C_{18}H_{18}O_6$	6626-61-5	
2	Lauryldiethanolamine	$C_{16}H_{35}NO_2$	1541-67-9	
3	Des-O-Methylasiodiplodin	$C_{16}H_{22}O_4$	32885-82-8	
4	Butyl isobutyl phthalate	$C_{16}H_{22}O_4$	17851-53-5	
5	Dibutyl phthalate	$C_{16}H_{22}O_4$	84-74-2	
6	Absciscic acid	$C_{15}H_{20}O_4$	21293-29-8	
7	Oleamide	$C_{18}H_{35}NO$	301-02-0	
8	2-Hydroxycinnamic acid	$C_9H_8O_3$	583-17-5	
9	Disobutyl phthalate	$C_{16}H_{22}O_4$	84-69-5	

(Continued)

**Table 2** (Continued).

Number	Compounds	Formula	CAS	Structure
10	Danthron	C <sub>14</sub> H <sub>8</sub> O <sub>4</sub>	117-10-2	
11	Embelin	C <sub>17</sub> H <sub>26</sub> O <sub>4</sub>	550-24-3	
12	Azelaic acid	C <sub>9</sub> H <sub>16</sub> O <sub>4</sub>	123-99-9	
13	Vertixanthone	C <sub>15</sub> H <sub>10</sub> O <sub>5</sub>	120461-93-0	

### GELNVs Active M1 Polarization of Macrophages

Given that M2-type microglia are prevalent near gliomas and promote their growth,<sup>39</sup> we investigated the role of GELNVs in the immune process (Figure 7A). Our analysis confirmed that GELNVs selectively influence M2 polarization in BV2 cells, as evidenced by flow cytometry detection of the M1 marker CD86 and the M2 marker CD206. Co-culture with GL261 cells or treatment with M2-conditioned IL-4 typically increased CD206 expression in BV2 cells while reducing CD86 levels. However, GELNVs treatment significantly decreased the M2/M1 ratio ( $p < 0.05$ , Figure 7B and C).

Additionally, we evaluated NO secretion capacity ( $p < 0.01$ , Figure 7D) and the mRNA expression levels of M1/M2 macrophage-associated markers and pro-inflammatory cytokines across the different groups ( $p < 0.01$ , Figure 7E–I). The results demonstrated that pre-treatment with GELNVs significantly increased the levels of the inflammatory mediator NO and upregulated mRNA expression of pro-inflammatory mediators, including iNOS, IL-1 $\beta$ , IL-6, and TNF- $\alpha$ , while downregulating the expression of the M2 macrophage polarization marker Arg-1. Collectively, these findings suggest that GELNVs play a crucial role in suppressing glioma growth and inhibiting M2 macrophage polarization within gliomas.

### Discussion

MEPNs can bind to drugs through endocytosis or receptor-mediated mechanisms, enabling efficient penetration of the blood-brain barrier while bypassing the P-glycoprotein (P-gp) drug efflux system, thereby achieving stable and prolonged drug delivery.<sup>15,40</sup> Furthermore, the extraction process of MEPNs does not involve organic solvents and leaves no toxic residues.<sup>41</sup> Collectively, MEPNs demonstrate superior biocompatibility, long-distance targeting capability, in vivo stability, and bioavailability compared to natural compounds extracted from plants. Additionally, compared to animal-derived exosomes, MEPNs possess distinct advantages including readily available raw materials, low production costs, and environmental sustainability,<sup>42</sup> as exemplified in this study by GELNVs derived from agricultural-waste mangosteen peel. MEPNs have garnered significant attention for their anti-tumor effects, primarily through mechanisms such as cell



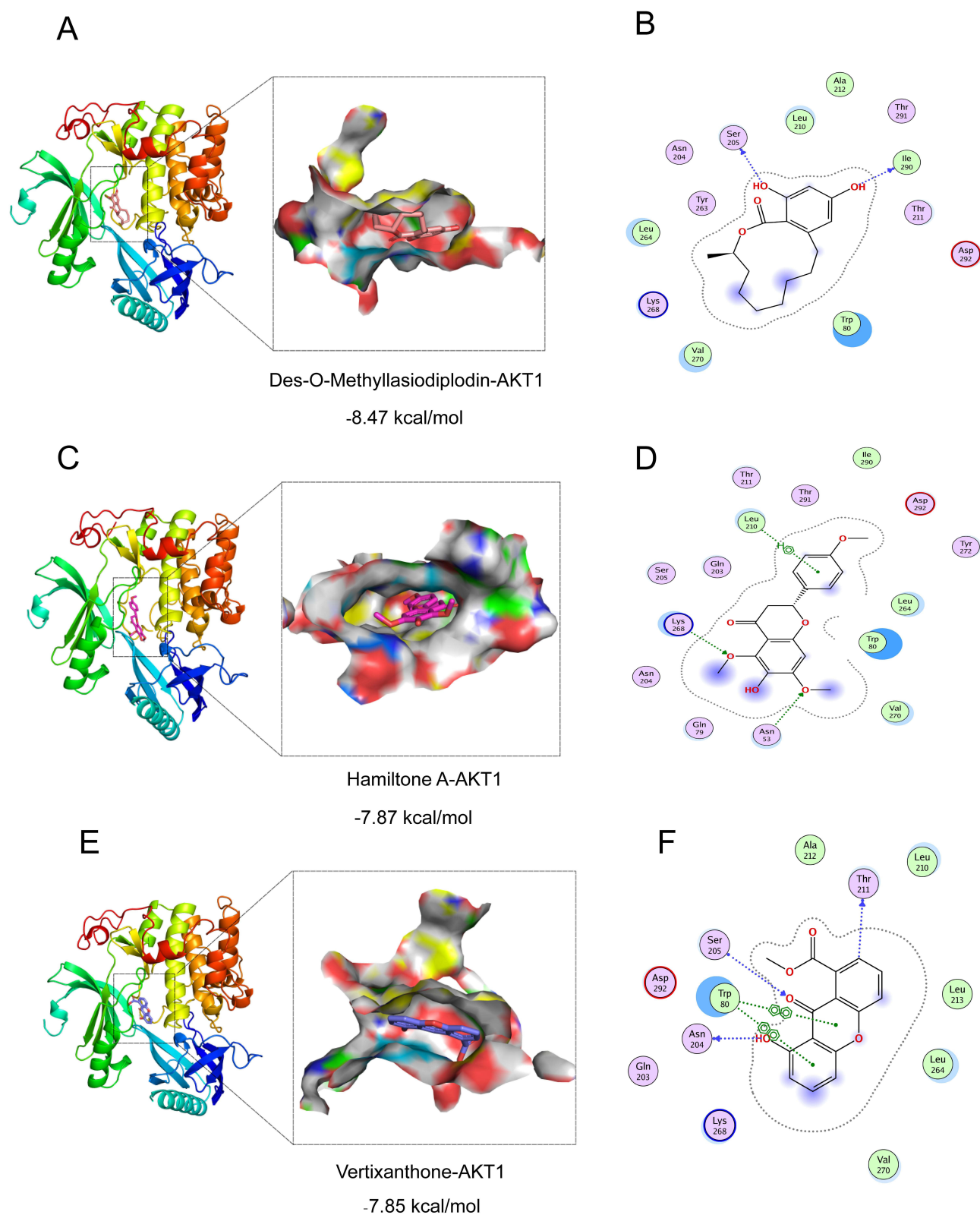


**Figure 5** Docking results of active compounds and the core targets. 3D and 2D visualization of molecular docking of AKT1 protein with Hamilton A (**A** and **B**) Des-O-Methylasiodiopodin (**C** and **D**) and Vertexanthone (**E** and **F**).

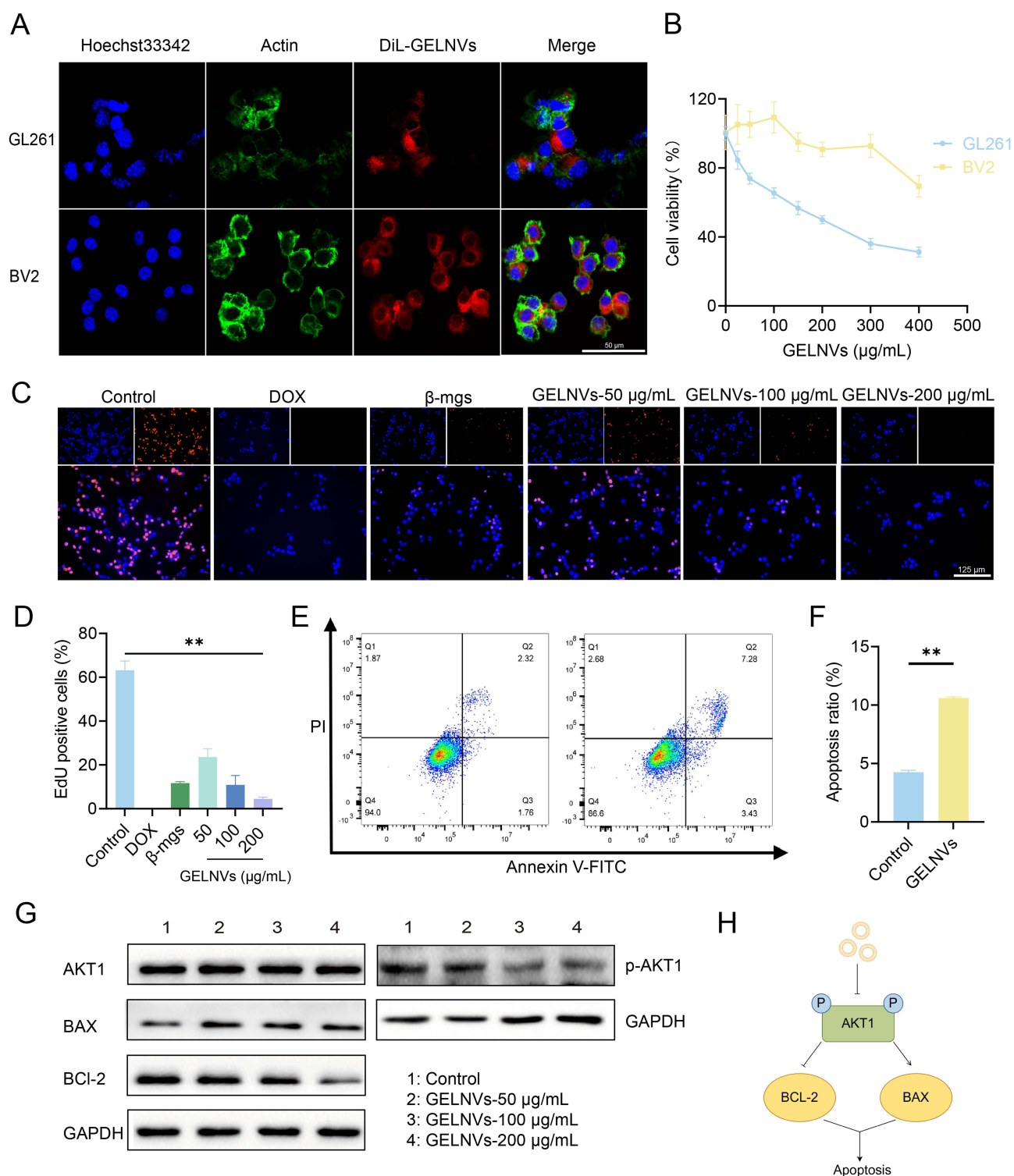


**Figure 6** Apoptosis in GL261 glioma cells treated with GELNVs and cellular uptake of GELNVs. **(A)** Confocal fluorescence imaging showed the internalization of GELNVs. After incubating GL261 and BV2 cells with DiI-labeled GELNVs for 24 hours, the distribution of GELNVs was assessed, scale bars=100  $\mu\text{m}$ . **(B)** Viabilities of BV2 cell and GL261 cell with the treatment of GELNVs for 24h. **(C)** Representative fluorescence microscopy images of GL261 cells stained with EdU after 24 hours of DOX,  $\beta$ -mgs, and GELNVs treatment, scale bars=125  $\mu\text{m}$ . **(D)** Quantification of the ratio of EdU-positive cells in GL261 cells. **(E and F)** Representative images of flow cytometry analysis for apoptosis using annexin V/propidium (PI) dual-labelling. **(G)** Western blotting analysis of the expression levels of BAX, BCL-2, AKT1 and p-AKT1 in GL261 cells receiving the treatment of GELNVs for 24h. **(H)** Schematic diagram of GELNVs inducing apoptosis in glioblastoma cells by inhibiting the AKT1 phosphorylation-dependent pathway. The result was compared with control groups, with significance levels indicated as \*\*  $p < 0.01$ ,  $n=3$ .

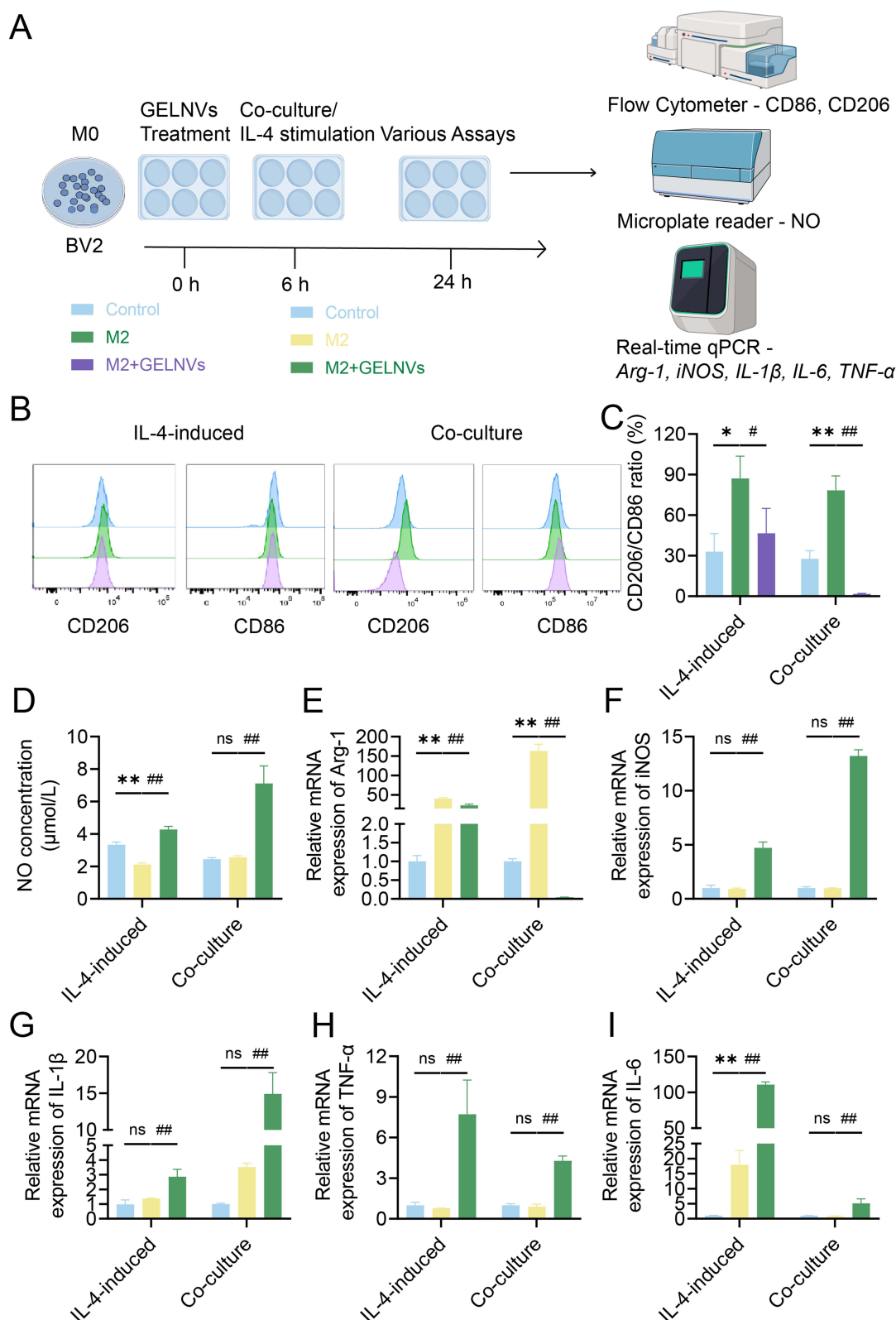


**Figure 7** GELNVs inhibit M2 polarization in BV2 cells. **(A)** Schematic diagram of M2-type macrophages treated with GELNVs. **(B and C)** Effects of GELNVs on CD206 and CD86 expression in BV2 cells. **(D)** GELNVs promoted nitric oxide release from BV2 cells. **(E and F)** Effects of GELNVs on the mRNA transcription levels of M1/M2-type related genes in BV2 cells. **(G–I)** GELNVs increased the mRNA transcription levels of pro-inflammatory cytokine genes in BV2 cells. \* The results were compared with control groups, with significance levels indicated as \*  $p < 0.05$  and \*\*  $p < 0.01$ ; # The results were compared with M2 groups, with significance levels indicated as #  $p < 0.05$  and ###  $p < 0.01$ ,  $n=3$ .

cycle arrest and mitochondrial damage.<sup>19</sup> Furthermore, several studies have highlighted that MEPNs can regulate tumor growth by modulating tumor-associated macrophage polarization.<sup>43,44</sup> Our previous research demonstrated that  $\beta$ -mangostin, a xanthone compound extracted from *Garcinia mangostana* L., targets and suppresses glioma by activating the STING pathway and polarizing tumor-associated microglia.<sup>26</sup> However, it remains unclear whether GELNVs possess similar functional properties. This study utilized a comprehensive approach integrating metabolomics, network pharmacology, molecular docking, and experimental validation to investigate the chemical characteristics, evaluate the anti-glioma effects, and elucidate the underlying mechanisms of GELNVs. Our results indicate that GELNVs inhibit proliferation and induce glioma cell apoptosis via the PI3K-Akt signaling pathway, and promote the polarization of microglia towards the M1 phenotype.

Through metabolomics analysis, we identified the chemical composition of GELNVs and found that these nanoparticles are rich in various bioactive compounds, including  $\beta$ -mangostin, danthron, quercetin-3-o-alloside, embelin, des-o-methylasiodiplodin, hamiltone A, and oleamide. These compounds likely work in synergy, collectively enhancing the therapeutic potential of GELNVs' anti-tumor effects.<sup>45–48</sup> Similar studies have shown that cucumber-derived nanovesicles containing cucurbitacin B exhibit potent tumor-suppressing capabilities, positioning them as a promising therapeutic option for non-small cell lung cancer treatment.<sup>49</sup> Likewise, sulforaphane compounds found in broccoli-derived nanoparticles have been demonstrated to effectively inhibit the progression of various cancers. Knockout and knock-in experiments with sulforaphane have validated its significant role in mediating the biological effects of PELNs.<sup>50,51</sup> These findings support the notion that MEPNs inherit the therapeutic properties of their source plants and contain bioactive compounds with potential in cancer treatment, positioning GELNVs as promising candidates for glioma therapy.

To explore the underlying mechanisms, we employed network pharmacology, identifying 10 key genes associated with cell proliferation, including AKT1, CTNNB1, EGFR, CASP3, BCL-2, CCND1, ERBB2, MMP9, PTGS2, and PPARG. These genes are involved in critical processes such as tumor cell proliferation, invasion, metastasis, angiogenesis, and apoptosis inhibition.<sup>52–55</sup> Among them, AKT1 was identified as the most crucial target, suggesting a pivotal role in GELNVs' anti-glioma mechanism. Molecular docking results revealed that des-o-methylasiodiplodin, hamiltone A, and vertexanthone exhibited strong binding affinities with AKT1. Both hamiltone A and vertexanthone, being flavonoids, demonstrated similar binding scores, likely due to their shared parent ring structures. AKT1 encodes a serine/threonine protein kinase, a critical component of the PI3K-Akt signaling pathway, which regulates multiple cellular functions, including cell survival, growth, and metabolism. AKT1 upregulation is closely related to the poor prognosis of glioma patients.<sup>56,57</sup>

To further verify the anti-glioma effects of GELNVs, we performed in vitro experiments on GL261 glioma cells. The results demonstrated that GELNVs significantly inhibited glioma cell proliferation and migration while promoting apoptosis, without exerting adverse effects on BV2 cells, exhibiting a larger therapeutic window compared to  $\beta$ -mangostin. Treatment with an AKT agonist was carried out to verify that GELNV induced apoptosis of glioma cells by activating the PI3K - Akt signaling pathway predicted by network pharmacology. Plant-derived exosomal vesicles from the traditional Chinese medicinal herb *Brucea javanica* (L). Merr. (BF-Exos) induce apoptosis in breast cancer cells through modulation of the PI3K/Akt/mTOR signaling pathway.<sup>12</sup> Therefore, the anti-tumor effects of GELNVs in other malignancies merit further exploration.

We also explored the effects of GELNVs on microglia polarization, as microglia play a crucial role in glioma progression. Cytokines secreted by glioma cells can activate microglia, thereby promoting tumor growth.<sup>58</sup> M1-type microglia secrete pro-inflammatory cytokines, proteinases, and reactive oxygen species, including NO, which exert toxic effects on glioma cells, contributing to their destruction.<sup>59,60</sup> Conversely, M2-type microglia promote glioma cell proliferation by secreting anti-inflammatory cytokines and suppressing anti-tumor immunity. Our data showed that GELNVs promoted M1-type microglia activation and inhibited the M2 polarization of BV2 cells, consistent with our previous research.

In conclusion, GELNVs have demonstrated the ability to regulate tumor cell growth and influence the polarization of tumor-associated microglia, making them a promising therapeutic strategy for glioma treatment. However, the present study has some limitations, most notably the lack of in vivo experimental validation. Although we have established the potential therapeutic effects and mechanisms of GELNVs in vitro, these predictions and findings need to be confirmed in

more complex biological systems. Future research should focus on in vivo experiments to further validate these mechanisms and explore the clinical relevance of GELNVs as a novel therapeutic approach for glioma treatment.

## Conclusion

This study represents the first attempt to extract exosome-like nanoparticles from *Garcinia mangostana* L., focusing on identifying the active ingredients in GELNVs that can be used to treat glioma. We demonstrated that GELNVs hold potential as a therapeutic strategy for glioma by inducing apoptosis in tumor cells and inhibiting their proliferation through the suppression of the PI3K-Akt signaling pathway. Additionally, we highlighted their potential role in modulating microglial polarization. These findings pave the way for the further utilization of *Garcinia mangostana* L. rind as a valuable resource and provide a solid foundation for future research into the anti-glioma effects of GELNVs.

## Highlights

- First study to extract exosome-like nanoparticles from *Garcinia mangostana* L. rind.
- Active components of GELNVs for glioma treatment explored through integrated strategy.
- GELNVs induce tumor cell apoptosis and inhibit proliferation via PI3K-Akt pathway.

## Abbreviations

BBB, blood brain barrier; DAVID, Database for Annotation, Visualization and Integrated Discovery; GELNVs, *Garcinia mangostana* L.-derived exosome-like nanoparticles; GO, Gene Ontology; IL-1 $\beta$ , interleukin-1 $\beta$ ; IL-4, interleukin-4; IL-6, interleukin-6; iNOS, inducible nitric oxide synthase; KEGG, Kyoto Encyclopedia of Genes and Genomes; MEPNs, medical and edible plant-derived nanovesicles; NO, nitric oxide; PBS, phosphate-buffered saline; PPI, protein-protein interaction; RCSB PDB, Research Collaboratory for Structural Bioinformatics Protein Data Bank; SDF, structure data file; SMILES, simplified molecular input line entry system; STRING, Search Tool for the Retrieval of Interaction Gene/Proteins; TNF- $\alpha$ , tumor necrosis factor- $\alpha$ .

## Ethics Statement

This research strictly adheres to international and domestic ethical guidelines and legal regulations governing the use of human data. Since the study utilized publicly available data with patient informed consent already obtained by the database provider, it was deemed exempt from additional ethical approval under the Measures for Ethical Review of Life Science and Medical Research Involving Human Subjects (China, 2023, Article 32, Items 1 and 2).

## Acknowledgments

This study was supported by Traditional Chinese Medicine Scientific Research Project of Zhejiang Province (2023ZL010) and Zhejiang Medical and Health Science and Technology Project (2022KY529, 2024KY636).

## Author Contributions

All authors made a significant contribution to the work reported, whether that is in the conception, study design, execution, acquisition of data, analysis and interpretation, or in all these areas; took part in drafting, revising or critically reviewing the article; gave final approval of the version to be published; have agreed on the journal to which the article has been submitted; and agree to be accountable for all aspects of the work.

## Disclosure

The authors declare that they have no known competing financial interests or personal relationships that could have appeared to influence the work reported in this paper.

## References

1. Altieri R, Agnoletti A, Quattrucci F. et al. Molecular biology of gliomas: present and future challenges. *Transl Med*. 2014;10:29–37. doi:10.1200/JCO.2008.19.8721



2. Poff A, Koutnik AP, Egan KM, Sahebjam S, D'Agostino D, Kumar NB. Targeting the Warburg effect for cancer treatment: ketogenic diets for management of glioma. *Semin Cancer Biol.* **2019**;56:135–148. doi:10.1016/j.semcancer.2017.12.011
3. Zhou YS, Wang W, Chen N, Wang LC, Huang JB. Research progress of anti-glioma chemotherapeutic drugs (Review). *Oncol Rep.* **2022**;47(5):101. doi:10.3892/or.2022.8312
4. Cao H, Li X, Wang F, Zhang Y, Xiong Y, Yang Q. Phytochemical-Mediated Glioma Targeted Treatment: drug Resistance and Novel Delivery Systems. *Curr Med Chem.* **2020**;27(4):599–629. doi:10.2174/0929867326666190809221332
5. Karachi A, Dastmalchi F, Mitchell DA, Rahman M. Temozolomide for immunomodulation in the treatment of glioblastoma. *Neuro Oncol.* **2018**;20(12):1566–1572. doi:10.1093/neuonc/noy072
6. Ortiz R, Perazzoli G, Cabeza L, et al. Temozolomide: an Updated Overview of Resistance Mechanisms, Nanotechnology Advances and Clinical Applications. *Curr Neuroparmacol.* **2021**;19(4):513–537. doi:10.2174/1570159X18666200626204005
7. Lim M, Xia Y, Bettegowda C, Weller M. Current state of immunotherapy for glioblastoma. *Nat Rev Clin Oncol.* **2018**;15(7):422–442. doi:10.1038/s41571-018-0003-5
8. Lin H, Liu C, Hu A, Zhang D, Yang H, Mao Y. Understanding the immunosuppressive microenvironment of glioma: mechanistic insights and clinical perspectives. *J Hematol Oncol.* **2024**;17(1):31. doi:10.1186/s13045-024-01544-7
9. Ye Z, Ai X, Yang K, et al. Targeting Microglial Metabolic Rewiring Synergizes with Immune-Checkpoint Blockade Therapy for Glioblastoma. *Cancer Discov.* **2023**;13(4):974–1001. doi:10.1158/2159-8290.CD-22-0455
10. Arcuri C. Microglia-glioma cross-talk a two way approach to new strategies against glioma. *Front Biosci.* **2017**;22(2):268–309. doi:10.2741/4486
11. Bai S, Wei Y, Liu R, Xu R, Xiang L, Du J. Role of tumour-derived exosomes in metastasis. *Biomed. Pharmacother.* **2022**;147:112657. doi:10.1016/j.biopha.2022.112657
12. Yan G, Xiao Q, Zhao J, et al. Brucea javanica derived exosome-like nanovesicles deliver miRNAs for cancer therapy. *J Control Release.* **2024**;367:425–440. doi:10.1016/j.jconrel.2024.01.060
13. Chronopoulos A, Kalluri R. Emerging role of bacterial extracellular vesicles in cancer. *Oncogene.* **2020**;39(46):6951–6960. doi:10.1038/s41388-020-01509-3
14. Li Y, Wang Y, Zhao H, Pan Q, Chen G. Engineering Strategies of Plant-Derived Exosome-Like Nanovesicles: current Knowledge and Future Perspectives. *Int J Nanomed.* **2024**;19:12793–12815. doi:10.2147/IJN.S496664
15. Dad HA, Gu TW, Zhu AQ, Huang LQ, Peng LH. Plant Exosome-like Nanovesicles: emerging Therapeutics and Drug Delivery Nanoplatfoms. *Mol Ther.* **2021**;29(1):13–31. doi:10.1016/j.ymthe.2020.11.030
16. Chen Q, Zu M, Gong H, et al. Tea leaf-derived exosome-like nanotherapeutics retard breast tumor growth by pro-apoptosis and microbiota modulation. *J Nanobiotechnology.* **2023**;21(1):6. doi:10.1186/s12951-022-01755-5
17. Ou X, Wang H, Tie H, et al. Novel plant-derived exosome-like nanovesicles from Catharanthus roseus: preparation, characterization, and immunostimulatory effect via TNF- $\alpha$ /NF- $\kappa$ B/PU.1 axis. *J Nanobiotechnology.* **2023**;21(1):160. doi:10.1186/s12951-023-01919-x
18. Yi Q, Xu Z, Thakur A, et al. Current understanding of plant-derived exosome-like nanoparticles in regulating the inflammatory response and immune system microenvironment. *Pharmacol Res.* **2023**;190:106733. doi:10.1016/j.phrs.2023.106733
19. Zhao B, Lin H, Jiang X, et al. Exosome-like nanoparticles derived from fruits, vegetables, and herbs: innovative strategies of therapeutic and drug delivery. *Theranostics.* **2024**;14(12):4598–4621. doi:10.7150/thno.97096
20. Zhao X, Yin F, Fu L, et al. Garlic-derived exosome-like nanovesicles as a hepatoprotective agent alleviating acute liver failure by inhibiting CCR2/CCR5 signaling and inflammation. *Biomater Adv.* **2023**;154:213592. doi:10.1016/j.bioadv.2023.213592
21. Kim J, Zhu Y, Chen S, et al. Anti-glioma effect of ginseng-derived exosomes-like nanoparticles by active blood-brain-barrier penetration and tumor microenvironment modulation. *J Nanobiotechnology.* **2023**;21(1):253. doi:10.1186/s12951-023-02006-x
22. Bai C, Liu J, Zhang X, et al. Research status and challenges of plant-derived exosome-like nanoparticles. *Biomed. Pharmacother.* **2024**;174:116543. doi:10.1016/j.biopha.2024.116543
23. Zhao Q, Feng J, Liu F, et al. Rhizoma Drynariae-derived nanovesicles reverse osteoporosis by potentiating osteogenic differentiation of human bone marrow mesenchymal stem cells via targeting ER $\alpha$  signaling. *Acta Pharmaceutica Sinica B.* **2024**;14(5):2210–2227. doi:10.1016/j.apsb.2024.02.005
24. Ovalle-Magallanes B, Eugenio-Pérez D, Pedraza-Chaverri J. Medicinal properties of mangosteen (*Garcinia mangostana* L.): a comprehensive update. *Food Chem Toxicol.* **2017**;109(Pt 1):102–122. doi:10.1016/j.fct.2017.08.021
25. Verma N, Pandit S, Kumar A, et al. Recent Update on Active Biological Molecules in Generating the Anticancerous Therapeutic Potential of *Garcinia mangostana*. *Appl Biochem Biotechnol.* **2022**;194(10):4724–4744. doi:10.1007/s12010-022-04031-2
26. Yang Y, Luo X, Wang Y, et al.  $\beta$ -Mangostin targets and suppresses glioma via STING activation and tumor-associated microglia polarization. *Biomed Pharmacother.* **2024**;177:117074. doi:10.1016/j.biopha.2024.117074
27. Wishart DS, Tzur D, Knox C, et al. HMDB: the Human Metabolome Database. *Nucleic Acids Res.* **2007**;35(Database):D521–D526. doi:10.1093/nar/gkl923
28. Zhu G, Wang S, Huang Z, et al. Rewiring of the Fruit Metabolome in Tomato Breeding. *Cell.* **2018**;172(1–2):249–261.e12. doi:10.1016/j.cell.2017.12.019
29. Gupta S, Rawat S, Arora V, et al. An improvised one-step sucrose cushion ultracentrifugation method for exosome isolation from culture supernatants of mesenchymal stem cells. *Stem Cell Res Ther.* **2018**;9(1):180. doi:10.1186/s13287-018-0923-0
30. Xu J, Yu Y, Zhang Y, et al. Oral administration of garlic-derived nanoparticles improves cancer immunotherapy by inducing intestinal IFN $\gamma$ -producing  $\gamma\delta$  T cells. *Nat Nanotechnol.* **2024**;19(10):1569–1578. doi:10.1038/s41565-024-01722-1
31. Liu J, Xiang J, Jin C, et al. Medicinal plant-derived mtDNA via nanovesicles induces the cGAS-STING pathway to remold tumor-associated macrophages for tumor regression. *J Nanobiotechnology.* **2023**;21(1):78. doi:10.1186/s12951-023-01835-0
32. Li W, Wen L, Chen Z, et al. Study on metabolic variation in whole grains of four proso millet varieties reveals metabolites important for antioxidant properties and quality traits. *Food Chem.* **2021**;357:129791. doi:10.1016/j.foodchem.2021.129791
33. NCBI. Absorption matters: a closer look at popular oral bioavailability rules for drug approvals - PubMed. <https://pubmed.ncbi.nlm.nih.gov/37550251/>. Accessed April 1, 2025.
34. NCBI. Study of Lipophilicity and ADME Properties of 1,9-Diazaphenothiazines with Anticancer Action - PubMed. <https://pubmed.ncbi.nlm.nih.gov/37108135/>. Accessed April 1, 2025.

35. Tran MN, Kim NS, Lee S. Biological network comparison identifies a novel synergistic mechanism of Ginseng Radix-Astragali Radix herb pair in cancer-related fatigue. *J Ethnopharmacol.* **2024**;333:118447. doi:10.1016/j.jep.2024.118447
36. Catania G, Rodella G, Vanvarenberg K, Pr  at V, Malfanti A. Combination of hyaluronic acid conjugates with immunogenic cell death inducer and CpG for glioblastoma local chemo-immunotherapy elicits an immune response and induces long-term survival. *Biomaterials.* **2023**;294:122006. doi:10.1016/j.biomaterials.2023.122006
37. Welsh JA, Goberdhan DCI, O'Driscoll L, et al. Minimal information for studies of extracellular vesicles (MISEV2023): from basic to advanced approaches. *J Extracell Vesicles.* **2024**;13(2):e12404. doi:10.1002/jev2.12404
38. Wang Y, Cheng D, He J, Liu S, Wang X, Wang M. Magnolol protects C6 glioma cells against neurotoxicity of FB1 via modulating PI3K/Akt and mitochondria-associated apoptosis signaling pathways. *Environ Pollut.* **2025**;372:126017. doi:10.1016/j.envpol.2025.126017
39. Vidyarthi A, Agnihotri T, Khan N, et al. Predominance of M2 macrophages in gliomas leads to the suppression of local and systemic immunity. *Cancer Immunol Immunother.* **2019**;68(12):1995–2004. doi:10.1007/s00262-019-02423-8
40. Saint-Pol J, Gosselet F, Duban-Deweer S, Pottiez G, Karamanos Y. Targeting and Crossing the Blood-Brain Barrier with Extracellular Vesicles. *Cells.* **2020**;9(4):851. doi:10.3390/cells9040851
41. Mu N, Li J, Zeng L, et al. Plant-Derived Exosome-Like Nanovesicles: current Progress and Prospects. *IJN.* **2023**;18:4987–5009. doi:10.2147/IJN.S420748
42. Ai S, Li Y, Zheng H, et al. Collision of herbal medicine and nanotechnology: a bibliometric analysis of herbal nanoparticles from 2004 to 2023. *J Nanobiotechnol.* **2024**;22(1):140. doi:10.1186/s12951-024-02426-3
43. Cao M, Yan H, Han X, et al. Ginseng-derived nanoparticles alter macrophage polarization to inhibit melanoma growth. *J Immunother Cancer.* **2019**;7(1):326. doi:10.1186/s40425-019-0817-4
44. Lv Y, Li M, Weng L, et al. Ginseng-derived nanoparticles reprogram macrophages to regulate arginase-1 release for ameliorating T cell exhaustion in tumor microenvironment. *J Exp Clin Cancer Res.* **2023**;42(1):322. doi:10.1186/s13046-023-02888-7
45. Nauman MC, Johnson JJ. The purple mangosteen (*Garcinia mangostana*): defining the anticancer potential of selected xanthenes. *Pharmacol Res.* **2022**;175:106032. doi:10.1016/j.phrs.2021.106032
46. Shi X, Zhang Y, Lin B, et al. Danthron attenuates experimental atherosclerosis by targeting foam cell formation. *Exp Physiol.* **2021**;106(3):653–662. doi:10.1113/EP089021
47. Zhou R, Lin ZH, Jiang CS, et al. Marine natural product des-O-methylsalsodiolin effectively lowers the blood glucose level in db/db mice via ameliorating inflammation. *Acta Pharmacol Sin.* **2013**;34(10):1325–1336. doi:10.1038/aps.2013.47
48. Zhou Y, Qian C, Tang Y, et al. Advance in the pharmacological effects of quercetin in modulating oxidative stress and inflammation related disorders. *Phytother Res.* **2023**;37(11):4999–5016. doi:10.1002/ptr.7966
49. Chen T, Ma B, Lu S, et al. Cucumber-Derived Nanovesicles Containing Cucurbitacin B for Non-Small Cell Lung Cancer Therapy. *Int J Nanomed.* **2022**;17:3583–3599. doi:10.2147/IJN.S362244
50. Chu K, Liu J, Zhang X, et al. Herbal Medicine-Derived Exosome-Like Nanovesicles: a Rising Star in Cancer Therapy. *Int J Nanomed.* **2024**;19:7585–7603. doi:10.2147/IJN.S477270
51. Deng Z, Rong Y, Teng Y, et al. Broccoli-Derived Nanoparticle Inhibits Mouse Colitis by Activating Dendritic Cell AMP-Activated Protein Kinase. *Mol Ther.* **2017**;25(7):1641–1654. doi:10.1016/j.ymthe.2017.01.025
52. Ma C, Feng Y, Zhong K, Wei J. PKM2 promotes glioma progression by mediating CTNNB1 expression. *Neurol Res.* **2024**;46(7):583–592. doi:10.1080/01616412.2024.2337508
53. Quesnel A, Coles N, Polvikoski TM, et al. The diagnostic and prognostic potential of the EGFR/MUC4/MMP9 axis in glioma patients. *Sci Rep.* **2022**;12(1):19868. doi:10.1038/s41598-022-24099-4
54. Saadeh FS, Mahfouz R, Assi HI. EGFR as a clinical marker in glioblastomas and other gliomas. *Int J Biol Markers.* **2018**;33(1):22–32. doi:10.5301/ijbm.5000301
55. Yu Y, Wang S, Wang Y, et al. AKT1 Promotes Tumorigenesis and Metastasis by Directly Phosphorylating Hexokinases. *J Cell Biochem.* **2024**;125(8):e30613. doi:10.1002/jcb.30613
56. Majewska E, Szeliga M. AKT/GSK3 $\beta$  Signaling in Glioblastoma. *Neurochem Res.* **2017**;42(3):918–924. doi:10.1007/s11064-016-2044-4
57. Wang Y, Xie X, Li S, et al. Co-overexpression of RIOK1 and AKT1 as a prognostic risk factor in glioma. *J Cancer.* **2021**;12(19):5745–5752. doi:10.7150/jca.60596
58. Wang XP, Guo W, Chen YF, et al. PD-1/PD-L1 axis is involved in the interaction between microglial polarization and glioma. *Int Immunopharmacol.* **2024**;133:112074. doi:10.1016/j.intimp.2024.112074
59. Lisi L, Laudati E, Navarra P, Dello Russo C. The mTOR kinase inhibitors polarize glioma-activated microglia to express a M1 phenotype. *J Neuroinflammation.* **2014**;11:125. doi:10.1186/1742-2094-11-125
60. Shen X, Burguillos MA, Osman AM, et al. Glioma-induced inhibition of caspase-3 in microglia promotes a tumor-supportive phenotype. *Nat Immunol.* **2016**;17(11):1282–1290. doi:10.1038/ni.3545